Applied Catalysis B: Environmental 188 (2016) 77–86

Contents lists available at ScienceDirect

Applied Catalysis B: Environmental

journal homepage: www.elsevier.com/locate/apcatb

Trichloroethene hydrodechlorination by Pd-Fe bimetallic nanoparticles: Solute-induced catalyst deactivation analyzed by carbon isotope fractionation

Yanlai Han [a], Changjie Liu [b], Juske Horita [b], Weile Yan [a,*]

[a] Department of Civil, Environmental, and Construction Engineering, Texas Tech University, Lubbock, TX 79409, USA
[b] Department of Geosciences, Texas Tech University, Lubbock, TX 79409, USA

ARTICLE INFO

Article history:
Received 31 August 2015
Received in revised form 13 January 2016
Accepted 19 January 2016
Available online 26 January 2016

Keywords:
Pd-Fe
Bimetallic iron
Hydrodechlorination
TriChloroethylene
Catalyst aging

ABSTRACT

Pd-Fe bimetallic nanoparticles (BNPs) have substantially higher reactivity for reductive dehalogenation of chlorinated ethenes (*e.g.*, trichloroethylene, TCE) compared to monometallic zero-valent iron nanoparticles, yet the rapid deactivation of BNPs in groundwater matrices limits their large-scale use in field applications. In spite of this shortcoming, the causes of BNP deactivation have not been clearly delineated. Stable carbon isotope fractionation measurements and product distribution analysis were used in this study to investigate the mechanisms of Pd-Fe deactivation in the presence of common groundwater solutes. Based on the apparent TCE degradation rates and at a constant solute concentration of 5 mM (except for humic acid, which was dosed at 20 mg/L), Pd-Fe BNPs exposed to SO_4^{2-}, HPO_4^{2-}, and humic acid solutions showed moderate declines in TCE dechlorination rates. Aging the bimetallic particles in Cl^-, SO_3^{2-}, HCO_3^-, and NO_3^- solutions, however, resulted in excessive or complete loss of TCE dechlorination reactivity. Analyses of the isotope fractionation associated with TCE hydrodechlorination (ε_{TCEHDC}) as well as the yield of ethane over other dechlorination products suggest at least four distinctive causes of deactivation: (i) aging the BNPs in deionized water and humic acid induces surface passivation due to buildup of mineral or organic carbon deposits; (ii) SO_3^{2-} and Cl^- ions interact specifically with Pd sites and disable the catalyst functions; (iii) NO_3^- and HCO_3^- inhibits iron corrosion, thereby limiting the production of H_2 as the precursor of reactive hydrogen species, and (iv) selective deactivation of surface sites involved in ethene hydrogenation was observed for BNPs aged in SO_4^{2-} and HPO_4^{2-} solutions. The findings suggest the Pd-on-Fe configuration of the bimetallic particles is susceptible to deactivation in a broader range of groundwater chemistry than previously expected.

1. Introduction

Catalytic hydrodechlorination (HDC) is an efficient and sustainable approach for the treatment of industrial wastewater or groundwater contaminated with chlorinated contaminants. Among many catalysts evaluated for this application, palladium is considered one of the most active metal for HDC reactions [1,2]. The prominent role of Pd stems from its ability in activating molecular hydrogen (H_2) to form reactive hydrogen species (*e.g.*, atomic hydrogen or hydride) [1,3] and efficient dissociation of carbon-chlorine bonds [4,5]. An important class of materials exemplifying Pd-catalyzed HDC is palladium-iron (Pd-Fe) bimetallic particles, in which a small amount of Pd is deposited onto zero-valent iron particles through a facile aqueous replacement reaction [6–8]. When colloidal or nanoscale iron is used, the resultant bimetallic nanoparticles (BNPs) can be directly injected into underground environment for *in situ* remediation of aquifers contaminated with chlorinated hydrocarbons [9,10].

Among many groundwater contaminants amenable to dehalogenation with Pd catalysts, chlorinated ethenes including trichloroethene (TCE) and tetrachloroethene (PCE) have received great attention because of their widespread occurrence at many U.S. superfund sites and their rapid transformation in the presence of Pd to completely dechlorinated products [2,11]. In contrast to chlorinated methanes or ethanes which undergo reduction via direct electron transfer, TCE or PCE reduction on metal surfaces involves an indirect reduction mechanism via reactive hydrogen species [12,13]. To enable *in situ* degradation of subsurface contaminants, a local source of H_2 is needed in the vicinity of Pd. As corrosion of iron in anoxic water produces

* Corresponding author.
E-mail address: weile.yan@ttu.edu (W. Yan).

http://dx.doi.org/10.1016/j.apcatb.2016.01.047
0926-3373/

hydrogen, a favorable synergy exists for Pd-Fe bimetallic material, where iron serves as the hydrogen source and catalyst support, and Pd acts as a catalyst for both hydrogen activation and HDC reactions. Indeed, rapid decomposition of chlorinated ethenes at rates thousand times that of the uncatalyzed iron have been documented in many laboratory investigations without forming the harmful chlorinated intermediates (*e.g.*, dichloroethenes or vinyl chloride) that are commonly observed in biological dehalogenation systems [14–16].

As with other metal catalysts, a serious impediment associated with the use of Pd is catalyst deactivation in the reaction media. Deactivation is particularly relevant to *in situ* groundwater remediation, as the aqueous phase typically contains substantial amounts of background electrolytes as well as dissolved organic carbon originated from natural decay processes. Typical inorganic solutes include chloride (Cl^-), sulfate (SO_4^{2-}), bicarbonate (HCO_3^-), nitrate (NO_3^-), and sulfide (HS^-), and their concentrations vary considerably with the site location, depth, and biogeochemical conditions. Among them, many are known to be potent deactivators of Fe [17,18] or Pd [19–21]. Not surprisingly, the Pd-Fe bimetallic nanoparticles have shown large susceptibility to solute-induced loss of reactivity [22,23]. In previous studies, particle deactivation was assessed by the rates of TCE degradation in batch experiments. Although bulk reaction rate is a useful indicator of the apparent effect of aqueous aging on particle reactivity, it offers limited insights into deactivation mechanisms caused by different groundwater solutes and the resultant impact on TCE degradation pathways.

Compound-specific isotope analysis (CSIA) is a valuable tool for assessing contaminant degradation in natural and laboratory environments [24–27]. The kinetic isotope effect (KIE) is built upon the principle that organic molecules with heavier isotopes generally experience slower bond breakage and thus, the heavier isotope tends to accumulate in the parent compound during the course of a degradation process. Consequently, an important application of CSIA is to assess the extent of contaminant transformation in an open system, since non-destructive loss of contaminants at a field site due to processes such as volatilization, sorption, diffusion, or dilution would contribute little to the isotope fractionation [25,28]. When applied in a controlled environment, isotope fractionation is useful to diagnose contaminant reaction pathways. It has been reported that abiotic dechlorination of PCE and TCE mediated by Fe(II)-containing minerals (*e.g.*, green rust, magnetite, or pyrite) [29] or zerovalent iron [15,30,31] is associated with more negative carbon isotope enrichment factors than biotic dechlorination processes [16]. Liang et al. attributed the suppressed isotope fractionation in biotic degradation to an increasing control of the degradation rates by mass transfer or complexation processes [16], which is analogous to the masking effect encountered in abiotic catalytic conversion reactions [32]. Elsner et al. observed that during abiotic dechlorination of dichloroethanes on Zn(0), the carbon isotope fractionation associated with β-dichloroelimination was much greater than the fractionation incurred during hydrogenolysis or α-elimination [33], thus the isotope data can be used to identify plausible mechanisms of the rate-limiting reactions. In a bimetallic system, iron and palladium need to work cooperatively in order to attain optimal HDC efficiency, thus the cause of particles deactivation is potentially more complex than monometallic iron. It is expected that CSIA combined with bulk kinetic and product speciation analyses would enable us to delineate the different mechanisms of catalyst deactivation in different groundwater matrices.

The objective of this study is to investigate the effects of common groundwater anions or natural organic matter on the reactivity of Pd-BNPs in TCE dechlorination reaction and to identify major factors contributing to the loss of reactivity or change in reaction pathways. Specifically, freshly made and various aged Pd-Fe BNPs (*i.e.*, particles pre-exposed to solutions containing different groundwater anions or natural organic carbon) will be evaluated in batch TCE hydrodechlorination experiments. The carbon isotope fractionations of TCE and daughter products were analyzed simultaneously using gas chromatography with a combustion isotope ratio mass-spectrometer (GC-C-IRMS) to quantify the TCE bulk enrichment factor (ε_{bulk}) and product-specific isotope fractionation values. Interpreting isotope effects together with kinetic data and product distribution allows insights to be gained into specific processes responsible for the declines in catalyst activity in different aqueous environment. This knowledge would serve to better predict and improve the performance of bimetallic material under environmentally relevant conditions.

2. Materials and methods

2.1. Preparation of nanoparticles

Nanoscale zero-valent iron (nZVI) particles were synthesized via borohydride reduction of an aqueous solution of ferric ions. Briefly, 10.8 g of $FeCl_3{\cdot}6H_2O$ (Fisher) were dissolved in a 500-mL solution mixture of distilled de-ionized (DDI) water and ethanol (1:1, v/v). 500 mL of 0.4 M $NaBH_4$ solution (Acros Organics) was introduced to the ferric solution at approximately 17 mL/min under a vigorous mixing condition, during which the ferric solution turned black due to the formation of colloidal-sized iron particles. The particles formed were collected by vacuum filtration and were stored in ethanol for further use. Pd-Fe bimetallic nanoparticles (denoted as Pd-Fe BNPs) were prepared by immersing the freshly prepared nZVI with an ethanol/water (1:1, v/v) solution of palladium chloride (Acros Organics) and ultrasonicating the mixture for 5 min [23]. The mass loading of Pd with respect to iron was fixed at 1.5% for all Pd-Fe BNPs. DDI water used in all procedures, including particle synthesis, aging and TCE experiments, was deoxygenated by purging with N_2 for 30 min.

2.2. Aging experiments

Aging experiments were conducted in 250-mL amber glass vials containing 200 mL of deoxygenated solutions amended with a common groundwater solute at 1–5 mM. Stock solutions of chloride, bicarbonate, nitrate, phosphate, sulfate and sulfite were prepared from their sodium salts, respectively. Stock solution of humic acid (Sigma-Aldrich, used as received) was prepared at 100 mg/L and was ultrasonicated for 10 min prior to use. The initial pH of the solutions was adjusted with dilute NaOH or HCl to between 7.4–8.2 to simulate the typical pH values encountered in groundwater. An appropriate amount of freshly made Pd-Fe BNPs was added into each solution at 2 g/L (dry weight) and the vial was sealed and agitated on a mechanical shaker for 24 h at room temperature ($22 \pm 1\,^{\circ}C$). The aged particles were collected by vacuum filtration and were used immediately in TCE degradation experiments.

2.3. TCE experiments and analytical method

TCE dechlorination experiments were performed to compare the reactivity of fresh and aged Pd-Fe BNPs. All batch experiments were conducted in 250-mL amber glass vials containing 200 mL of aqueous solution and the balance as headspace. Experiments were performed with fresh or aged nanoparticles added at 1–5g/L (dry weight). The vials were capped with Teflon Mininert valves, spiked with a small aliquot of TCE stock solution (in methanol and amended with 2-propanol as an internal standard), and placed on a wrist-action shaker at 250 rpm at room temperature. To monitor the concentrations and carbon isotope ratios of TCE and the reaction

products, headspace samples (200–500 μL) were manually withdrawn and injected to a gas chromatograph-combustion-isotope ratio mass spectrometer (GC-C-IRMS) system periodically using a gastight syringe. The system comprised of TRACE GC Ultra (Thermo Scientific) installed with a PoraPlot Q capillary column (Varian, #CP7551) and GC Isolink (Thermo Scientific) coupled with ConFlo IV (Thermo Scientific) and Delta V IRMS (Thermo Scientific). The GC temperature program ramped the oven from 35 °C to 220 °C in 26 min, with a 4 min hold at 35 °C. The flow rate of He carrier gas was set at 1.2 mL/min with split ratio of 8. TCE and the reaction products were separated by the GC column, and then oxidized into CO_2 by GC Isolink at 1030 °C. The CO_2 produced by each analyte was introduced to IRMS for carbon isotope ratio analysis. Based on IRMS signal intensities, the concentrations of TCE and reaction products in the headspace samples were determined using calibration curves constructed with the corresponding commercial standards. Their concentrations in the solution phase were deduced from their concentrations in the headspace using Henry's Law constants [34]. Carbon isotope ratios are reported as $\delta^{13}C$ following Eq. (1):

$$\delta^{13}C(‰) = (R_{sample}/R_{standard} - 1) \times 1000 \quad (1)$$

where R_{sample} is the $^{13}C/^{12}C$ ratio of a given sample and $R_{standard}$ is the $^{13}C/^{12}C$ ratio of the international standard reference material, V-PDB [35,15]. TCE and the reaction products were analyzed for $\delta^{13}C$ values relative to a reference CO_2 gas, and then normalized to the V-PDB scale against NG2 standard [36].

2.4. Evaluation of isotope fractionation

Isotope fractionation associated with a chemical reaction is represented by an isotope fractionation factor (α), which is defined as in Eq. (2),

$$\alpha = \frac{^{h}k}{^{l}k} \quad (2)$$

where ^{h}k and ^{l}k are the rate constants of a chemical reaction involving a substrate containing the heavier and lighter isotope (in this case, ^{13}C and ^{12}C), respectively. Applying Eq. (2) into a relevant kinetic expression and integrating over the extent of the reaction yield the Rayleigh equation (Eq. (3)), where R_o and R stand for the isotope ratio of a substrate at the beginning of a reaction and at a given time, respectively. f is the fraction of the substrate remain at the specified time.

$$R/R_o = f^{(\alpha-1)} \quad (3)$$

The isotope fractionation factor is related to the apparent enrichment factor, ε_{bulk}, as in Eq. (4).

$$\varepsilon_{bulk}(‰) = (\alpha - 1)\,1000 \quad (4)$$

Note that in deriving the Rayleigh equation, one assumes that the reaction itself is rate-limiting. This is not necessarily the case in catalytic reactions, where previous steps such as mass diffusion and adsorption of a substrate to reactive sites may proceed irreversibly or be rate-controlling. Since these preceding steps carry a negligible or minor isotope fractionation effect, ε_{bulk} may exhibit a small value that does not reflect the intrinsic isotope effect of the reaction. In such case, the isotope effect of a reaction can be estimated from the change in $\delta^{13}C$ of the substrate and product at the initial stage of the experiments, when accumulation of product is considered negligible [15]. If multiple products are formed simultaneously or a product undergoes rapid further transformation steps, an average isotope value weighted by the molar ratio of the respective products may be used. In the case of TCE, the calculation of ε_{TCEHDC} is described in Eq. (5), where $\delta^{13}C_{productave,0}$ and

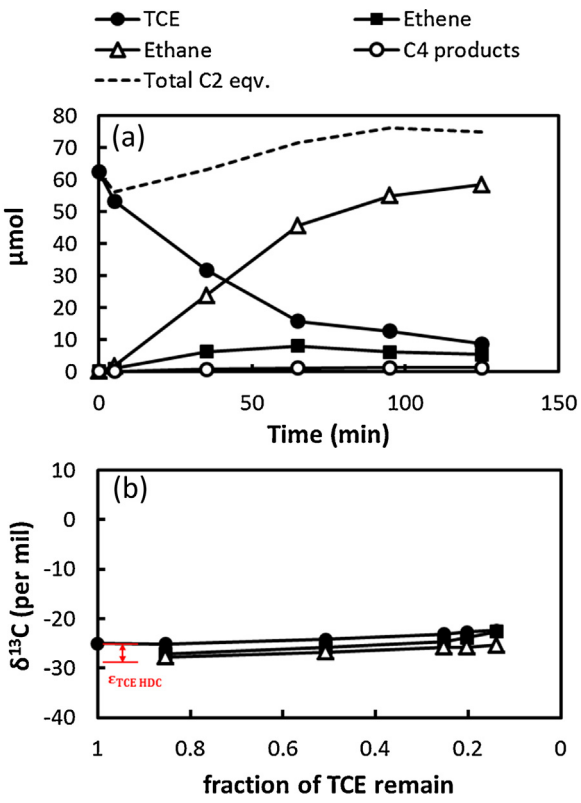

Fig. 1. (a) Reductive dechlorination of TCE by fresh Pd-Fe nanoparticles and (b) changes in $\delta^{13}C$ values of TCE and reaction products during the experiment. Nanoparticle dose was 1 g/L.

$\delta^{13}C_{TCE,0}$ represent the average isotope composition of the products (predominantly, ethene and ethane) and the substrate at the initial stage of an experiment:

$$\varepsilon_{TCEHDC} = \delta^{13}C_{productave,0} - \delta^{13}C_{TCE,0} \quad (5)$$

ε_{bulk} and ε_{TCEHDC} differ in the sense that ε_{bulk} reflects the isotope fractionation of the rate-limiting step, whereas ε_{TCEHDC} accounts for the fractionation of all steps involved in converting TCE to the major products. Since mass transport and adsorption steps have considerably smaller isotope effects than chemical conversion, ε_{TCEHDC} is a good indicator of the intrinsic KIE of a reaction and it is not affected by the kinetic masking effect often encountered in catalytic reactions [35].

Lastly, possible isotopic fractionation due to the transfer of TCE between the aqueous and gaseous phases is a valid concern during headspace analysis. In this study, the carbon isotope ratios of TCE in a water free vial and TCE in the headspace of the controls were identical within analytical error (±0.47‰).

3. Results

3.1. TCE dechlorination by fresh Fe and Pd-Fe NPs

The reactivity of various Pd-Fe BNPs was evaluated using TCE batch experiments. Fresh Pd-Fe BNPs exhibited excellent reactivity with greater than 85% of TCE (C_o = 50 mg/L) degraded within 125 min (Fig. 1a). Chlorinated intermediates known to form during biological attenuation of TCE (*e.g.*, DCEs and VC) were not detected in the headspace samples, in agreement with previous studies that abiotic reduction of TCE on zero-valent metal surface favors the formation of completely dechlorinated hydrocarbons [15,37,38]. Ethane and ethene are the major products, accounting for 90% and 7.2%, respectively, of the total products formed at the last sampling

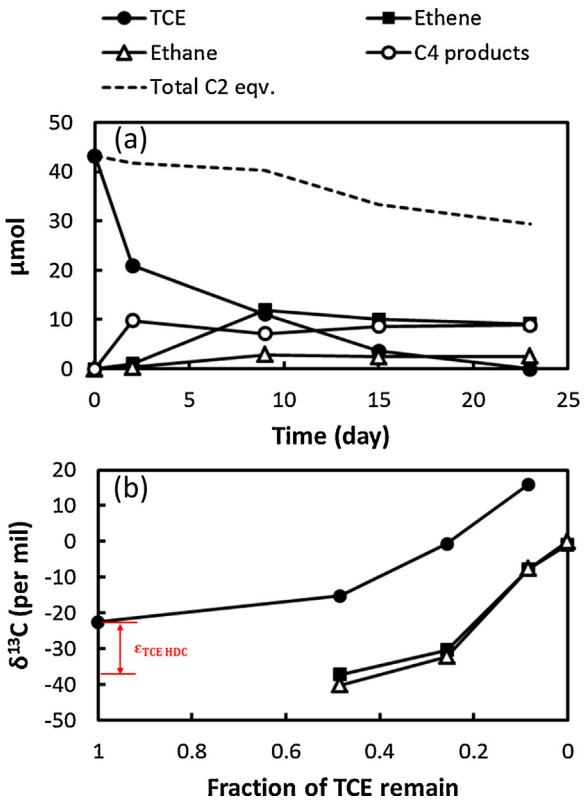

Fig. 2. (a) Reductive dechlorination of TCE by fresh Fe nanoparticles and (b) changes in $\delta^{13}C$ values of TCE and reaction products during the experiment. Nanoparticle dose was 5 g/L.

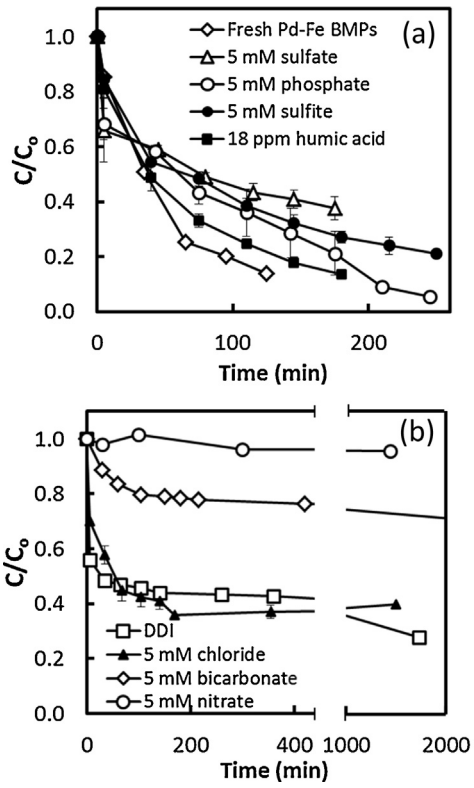

Fig. 3. TCE degradation by (a) fresh and moderately deactivated and (b) severely deactivated Pd-Fe nanoparticles. Aging was conducted by immersing freshly made Pd-Fe in various aqueous solutions for 24 h prior to TCE experiments. Initial TCE concentration was 50 mg/L. Dose of Pd-Fe was 1 g/L and 2 g/L for fresh and aged particles, respectively.

point. The ratio of ethane to ethene increased with reaction time, indicating that the fresh Pd-Fe is capable of hydrogenating ethene. Ethene reduction is a distinct capability of the bimetallic particles since additional experiments showed that monometallic Fe nanoparticles were unable to convert ethene to ethane under similar conditions. A small amount of C_4 products (butane and butene isomers) was detected. Their combined concentration accounts for less than 4% of the total carbon, and trace levels of C_5–C_6 alkanes and alkenes were also detected but not quantified. These minor products suggest hydrocarbon coupling reactions had occurred to a small extent on Pd-Fe BNPs.

TCE reduction by monometallic Fe NPs (Fig. 2a) was considerably slower, requiring more than 10 days to degrade the equivalent amount of TCE converted by Pd-Fe in 2 h. Adding up TCE and product concentrations did not give a good carbon balance and this was attributed to sampling loss due to build-up of overpressure in the reaction vessel over a long monitoring period (23 days). Product analysis identified ethene and C_4 products to be the major products. C_4 products were formed primarily at the initial stage of the experiment. Ethane, in comparison, constitutes only 8.5% of the total products formed. Compared to Pd-Fe, monometallic Fe possesses significantly lower activity for hydrodechlorination (of TCE) and hydrogenation (of ethene) but a higher propensity to promote chain growth reactions. The latter property is in line with the prevalent use of iron as hydrocarbon synthesis or reforming catalysts (*e.g.*, in Fischer-Tropsch synthesis) [39,40].

Figs. 1 b and 2 b illustrate the isotopic composition of TCE and its daughter products with reaction time. Fitting the experimental data to the Raleigh model yields satisfactory fits (Fig. S1), thus we may consider that a constant isotope fractionation prevails during the experiment periods. Comparing the data of the Pd-Fe and Fe systems, several differences can be discerned. With Pd-Fe (Fig. 1b), TCE experienced little isotope fractionation during its rapid transformation, whereas TCE degradation by Fe NPs led to a strong enrichment of ^{13}C in the remaining TCE. The bulk enrichment factor, ε_{bulk}, of the two materials was evaluated according to the Rayleigh equation (Eq. (3)) to be -1.4 ± 0.1‰ and -15.6 ± 2.3‰, respectively (Fig. S1). In prior studies, $\varepsilon_{bulk}$of TCE dechlorination was reported in a range of -10.1‰ to -24.8‰ for various commercial or research-grade zero-valent iron materials under laboratory or field conditions [41,30,42]. For nanoscale iron, $\varepsilon_{bulk}$was reported at approximately -20.9‰ [15], which is higher than the value obtained in this study (-15.6 ± 2.3‰), but within the range mentioned above for a wide variety of iron materials. The discrepancy in ε_{bulk} may stem from difference in the surface properties of iron used in different studies as well as possible transport limitation in some column experiments. Compared to monometallic Fe, bulk enrichment factor of TCE degradation by Pd-Fe is characteristically small. The greatly diminished isotope effect is often interpreted as due to a kinetic masking effect, in which accelerated surface reactions in the presence of a catalyst cause the preceding less-fractionating steps (*i.e.*, transport of reactant from the bulk solution to the surface and adsorption to reactive sites) to be more rate-limiting [35]. Another explanation is that smaller TCE fractionation on Pd-Fe BNPs is resulted from a decrease in the kinetic isotope effect (KIE) of TCE reduction due to facilitated bond-breaking on the catalyst surface. Using Eq. (5), $\varepsilon_{TCEHDC}$is estimated to be -2.5‰ and -13.7‰, respectively, for Pd-Fe and the monometallic Fe. The results imply that TCE transformation on the bimetallic surface incurs a much smaller intrinsic kinetic isotope effect than its reaction on Fe particles. It was postulated in previous studies that abiotic reduction of unsaturated chlorinated compounds on metal surface is preceded by the formation of a strong precursor complex [2,43,44]. Spectroscopic investigations suggest the C—Cl bonds of chlorinated ethenes were

Table 1
Pertinent kinetic, isotopic, and production distribution parameters of TCE hydrodechlorination reactions with fresh and aged Pd-Fe BNPs.

Solution	k_m (10^{-2} L g^{-1} min^{-1})[a]	ε_{bulk}	ε_{TCEHDC}	Ethane Selectivity[d]
Fe nanoparticles	$(2.15 \pm 0.64) \times 10^{-3}$	-15.8 ± 2.6	-13.7	0.08
Fresh Pd-Fe	1.37 ± 0.68	-1.6 ± 0.2	-2.5	0.88
Pd-Fe aged in DDI	N.D.[b]	-4.6 ± 0.7	-2.8	0.54
Pd-Fe aged in 20 mg/L HA	0.37 ± 0.08	-4.9 ± 1.2	-6.0	0.70
Pd-Fe aged in 5 mM Cl^-	N.D.[b]	-10.8 ± 2.5	-14.0	0.12
Pd-Fe aged in 5 mM SO_3^{2-}	0.24 ± 0.03	-12.6 ± 0.1	-14.3	0.23
Pd-Fe aged in 5 mM SO_4^{2-}	0.12 ± 0.03	-6.5 ± 1.6	-15.0	0.29
Pd-Fe aged in 5 mM HPO_4^{2-}	0.55 ± 0.04	-6.8 ± 1.5	-10.0	0.29
Pd-Fe aged in 1 mM HCO_3^-	N.D.[b]	N.D.[c]	-0.5	0.57
Pd-Fe aged in 1 mM NO_3^-	N.D.[b]	N.D.[c]	-2.3	0.58

[a] Estimated by fitting experimental data (t > 35 min) to pseudo-first-order kinetic model.
[b] Not determined (N.D.) due to severe deviation from pseudo-first-order kinetics.
[c] Not determined (N.D.) due to limited TCE conversion and poor fits to the Raleigh equation (Fig. S3).
[d] Estimated from ethane produced over total product formation at ~90% conversion of TCE or the last sampling point for strongly deactivated particles.

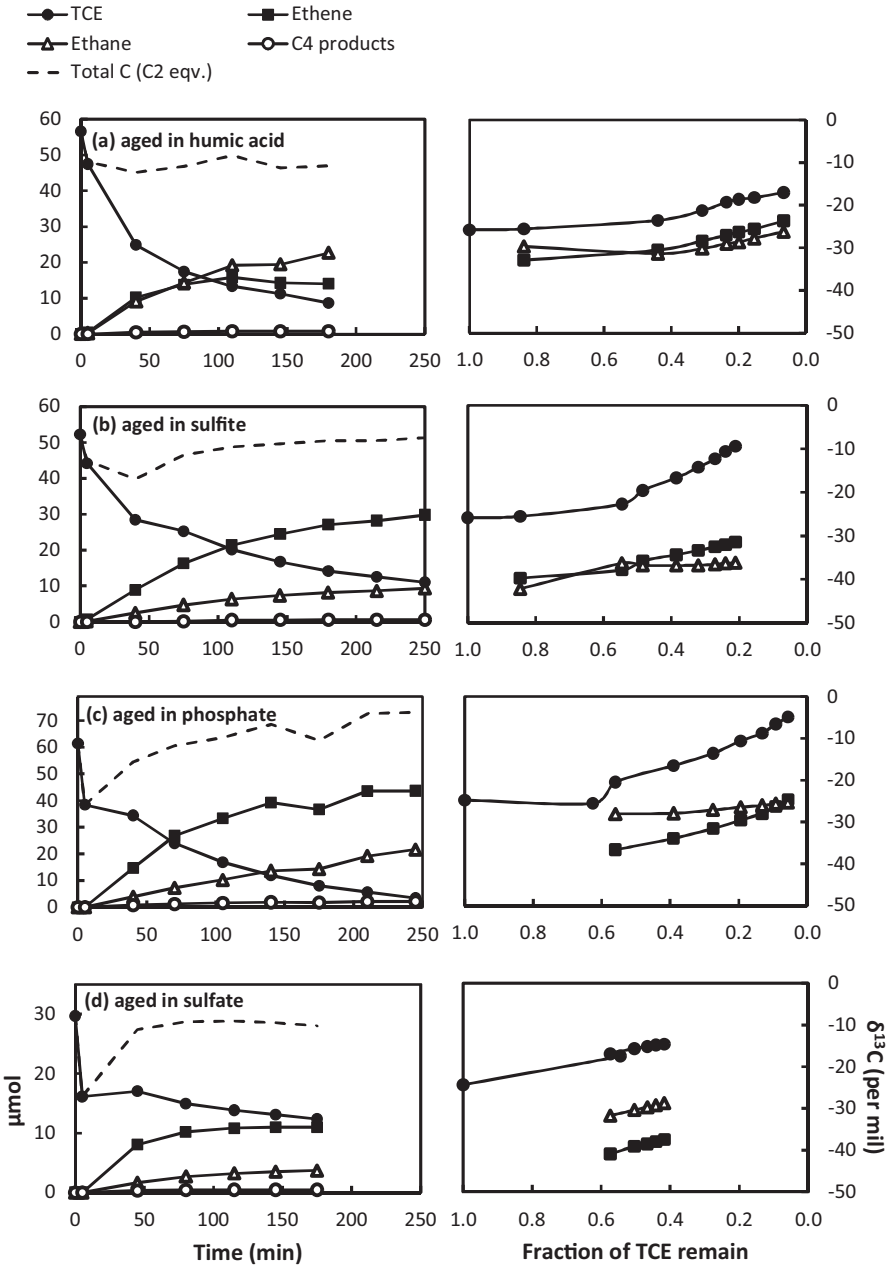

Fig. 4. Product distribution and carbon isotope fractionation during TCE degradation by Pd-Fe aged in the presence of (a) 20 mg/L humic acid, (b) 5 mM sulfite, (c) 5 mM phosphate, and (d) 5 mM sulfate. The initial pH of the aging solutions was in the range of 7.4–8.2.

significantly weakened upon adsorption of the reactant on the Pd surface [5,45]. This thus explains the substantially reduced kinetic isotope effect during TCE conversion on fresh Pd-Fe nanoparticles. Lastly, the isotope discrimination between ethene and ethane are relatively small in both Fe and Pd-Fe systems, a result as expected since hydrogenation of carbon double bonds should invoke a minor isotope effect on the participating carbon atoms [31].

3.2. TCE dechlorination by aged Pd-Fe NPs

Fig. 3 shows TCE dechlorination by Pd-Fe nanoparticles that had been pre-exposed to different solution environment for 24 h prior to TCE experiments. On the basis of TCE removal rate, the aged Pd-Fe BNPs exhibit two types of deactivation behavior. As shown in Fig. 3(a), particles aged in 5 mM of sulfite, sulfate, and phosphate and humic acid (at 20 mg/L) suffered moderate degrees of reactivity loss compared to the fresh Pd-Fe BNPs. Their apparent mass-normalized pseudo first-order rate constants (k_m) were approximately one order of magnitude lower than that of the fresh Pd-Fe BNPs (Table 1). In comparison, particles aged in DDI or 5 mM of chloride (Cl^-), bicarbonate (HCO_3^-), and nitrate (NO_3^-) show signs of severe deactivation. In several cases, there was an initial reduction in TCE concentration in 2 h, however, TCE conversion beyond the initial phase was virtually negligible. Continuous monitoring for up to 2 days suggests these particles were essentially unreactive. We attribute the initial rapid disappearance of TCE to its reaction with a limited amount of active H species accumulated on the catalyst during the aging process. This is supported by the observation that sonicating the aged particles in clean water for several minutes to release the surface bound hydrogen species followed by collecting the particles and placing them in TCE solutions resulted in negligible degradation of TCE even during the initial phase (Fig. S2).

Product distribution and carbon isotope analysis are used here to further investigate the deactivation mechanisms. Results of BNPs aged in four moderately deactivating solutions are shown in Fig. 4. Pertinent parameters, including k_m, ε_{bulk}, and ε_{TCEHDC} are summarized in Table 1. The Table also lists ethane selectivity, which is defined as the amount of ethane produced over the total product formation at approximately 90% TCE conversion or, in the case of incomplete conversion due to strong deactivation, at the last sampling point. In spite of similar TCE degradation rates (Fig. 3a), values of ε_{TCEHDC} and ethane selectivity are remarkably different in these reaction systems. Specifically, Pd-Fe aged in humic acid exhibits a relatively small ε_{TCEHDC} and the highest ethane selectivity among the aged Pd-Fe particles (Fig. 4a). On the other hand, a large isotope depletion was observed in the case of sulfite-aged particles along with a small ethane selectivity (Fig. 4b), implying that the deactivation effect of sulfite ions is specific to the Pd surface. The BNPs aged in phosphate and sulfate solution demonstrate intermediate shifts in ethane selectivity. However, unlike particles aged in sulfite or humic acid in which ethene and ethane experienced similar extents of isotope enrichment, $\delta^{13}C$ of the two hydrocarbon products formed in the presence of sulfate or phosphate-aged particles differ considerably (Fig. 4c and d). Based on this data, it can be reasoned that ethene is not a precursor of ethane. Rather, independent pathways are involved in the formation of ethene and ethane at possibly different reactive sites on the particles aged in sulfate or phosphate solutions. With phosphate-aged BNPs, ethane undergoes negligible isotope fractionation during its formation, and its isotope ratio is similar to that of the original TCE. In comparison, there is a large isotope depletion during TCE conversion to ethene. These characteristics infer that ethane formation involves predominantly Pd surface while the production of ethene was associated with Fe sites. The conversion of ethene to ethane, a facile process by fresh Pd-Fe BNPs, is severely blocked on particles aged in phosphate and sulfate solutions.

Fig. 5 shows the isotope fractionation and product formation during TCE degradation by particles aged in four strongly deactivating solutions, namely DDI, chloride, bicarbonate, and nitrate. With BNPs aged in DDI (Fig. 5a), 40% of TCE was removed in the first 5 min, however, the loss was not accompanied by quantitative formation of dechlorination products, suggesting the initial loss of TCE is due to non-reactive sorption to the solid phase [46]. Of the limited amount of TCE transformed, the isotope discrimination between TCE and dechlorination products is characteristically small ($\varepsilon_{TCEHDC} = -2.8$ ‰). On the contrary, particles aged in the chloride solution undergo substantial fractionation during TCE reduction (Fig. 5b). The highly negative ε_{TCEHDC} value of −14.0 ‰, comparable to the value of monometallic iron (−13.7‰), points to severe impairment of Pd activity by chloride ions. This observation is also supported by ethene being the predominant product in the chloride-aged BNP system. Due to limited conversion of TCE by Pd-Fe aged in 5 mM nitrate and bicarbonate solutions, we conducted isotope experiments using particles aged in 1 mM of each solute. The results, in Fig. 5c and d, show that, the reactions of TCE on bicarbonate- and nitrate-aged BNPs resulted in very small fractionations during both ethene and ethane production. Hence, the decline in reactivity cannot be attributed to deactivation of Pd sites.

pH change during TCE dechlorination reactions was monitored (Table S1). In general there is a moderate pH drop by 1–2 units after reactions with TCE, except in the case of Pd-Fe aged in DDI and 5 mM chloride during which pH decreased by more than 4 units. This significant pH drift is attributed to enhanced iron corrosion as indicated by the release of a large amount of dissolved Fe during aging in DDI and chloride solutions (Fig. S4), given that hydrolysis of dissolved Fe can produce considerable acidity. The influence of pH on reactivity is two-fold: while lower pH accelerates H_2 production and favors TCE dechlorination from a stoichiometric point of view [47,48], Pd is less active at lower pH, particularly in the presence of chloride [11,49]. The net effect on Pd-Fe reactivity will likely differ for the particles aged in DDI and chloride solutions as discussed below.

4. Discussion

4.1. Solute-induced deactivation mechanisms

Pd catalysts have been extensively studied for catalytic decomposition of halogenated contaminants. Treatment of industrial wastewater or *ex situ* remediation of contaminated groundwater typically employ the catalyst with H_2 in continuous flow-through reactors. To apply Pd catalysts to *in situ* subsurface remediation, a sustained source of H_2 is required close to the contaminant reaction zone. One strategy to achieve this is to incorporate Pd onto zero-valent iron, where iron oxidation by water provides a continuous supply of H_2 that is subsequently activated by Pd surface [9,50]. Among the common solutes found in the subsurface environment, reduced sulfur species (*e.g.*, sulfite and sulfide ions) [2,19,51,52] and natural organic matter (NOM) [52,53] are known to exert strong deactivation effects on Pd reactivity. These observations agree on a large part with findings in the current study. A self-inhibitory effect has also been noted in the past, which is caused by the inhibition of Pd activity by the halogen ions produced during hydrodehalogenation reactions (*i.e.*, Cl^- or Br^-), and such effect is more severe in gas or solvent phase HDC reactions at elevated contaminant concentrations [20,54,55]. Results in this study demonstrate that chloride ions as a natural constituent in groundwater can induce a serious impairment of Pd activity when present at a significant level. No adverse effect was reported in solute-free water for other bimetal-

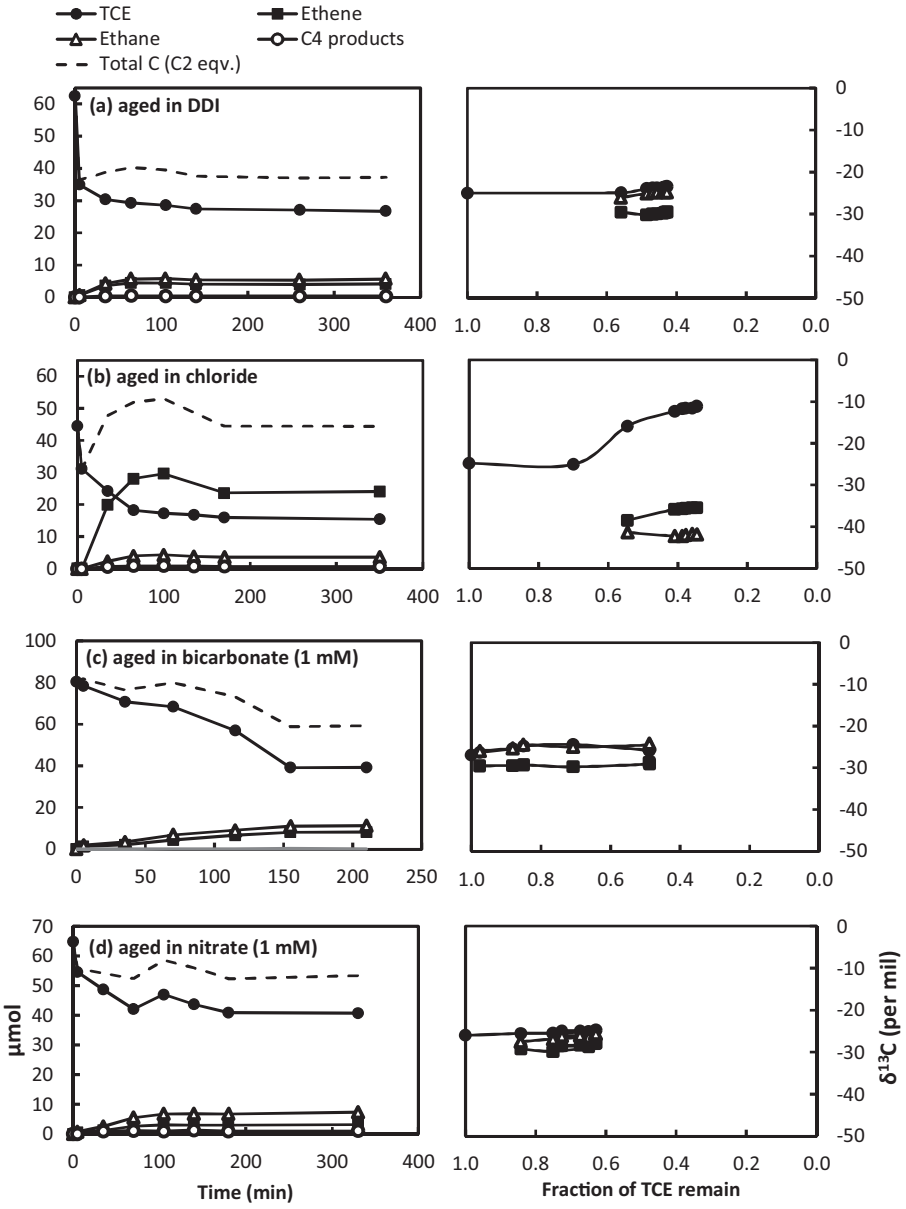

Fig. 5. Product distribution and carbon isotope fractionation during TCE degradation by Pd-Fe aged in the presence of (a) distilled deionized water (DDI), (b) 5 mM chloride, (c) 1 mM carbonate, and (d) 1 mM nitrate. The initial pH of the aging solutions was in the range of 7.4–8.2.

lic particles (*e.g.*, iron-supported nickel) [34] or Pd/H_2 systems [11], yet severe deactivation of Pd-Fe results upon immersion in deionized water. Prior surface and electron microscopic characterizations attributed this to the galvanic effect between the nanosized Pd deposits and the underlying Fe phase, leading to excessive iron corrosion in a short period of time (24 h) and the enclosure of Pd deposits by iron oxidation products [23,56]. Other common solutes such as bicarbonate, nitrate, and phosphate do not appreciably affect Pd activity in Pd/H_2 reactors [19], however, the current study shows that these anions slow down the reactivity of Pd-Fe BNPs to appreciable degrees.

Fig. 6a shows a conceptual model of TCE transformation on fresh Pd-Fe BNPs. It has been established previously that reductive dechlorination on zero-valent iron or in a Pd-catalyzed system are surface-mediated [57,58]. The reaction is initiated by the production of H_2 from Fe(0) corrosion and the adsorption of H_2 on the Pd surface to form dissociated hydrogen species. Subsequently, TCE reduction may occur via three pathways (as denoted by numbers in Fig. 6a). The first involves the adsorption of TCE at Pd sites followed by multiple surface reactions to form predominantly ethane, as was reported in previous studies [58]. In the second pathway, Fe itself is able to activate H_2 and mediate TCE degradation. This process is however remarkably slow (Fig. 2) and therefore does not contribute significantly to the observed TCE degradation within the time frame of investigation (<24 h). In the third pathway, we postulate migration of activated hydrogen from Pd to Fe sites, and TCE was degraded on the Fe surface. Spillover of atomic hydrogen from hydrogen dissociation catalysts such as palladium or platinum to support surface is well documented in heterogeneous catalytic reactions [59,60]. This process is considered kinetically facile at ambient temperature and has been proposed as an important pathway of Pd-catalyzed hydrodechlorination in the aqueous environment [1,61]. In this instance, Pd serves as an indirect catalyst by facilitating the accumulation of active hydrogen species on the Fe surface. It is difficult to differentiate pathway 1 and 3 unambiguously with kinetic data alone, however, the distinct isotope

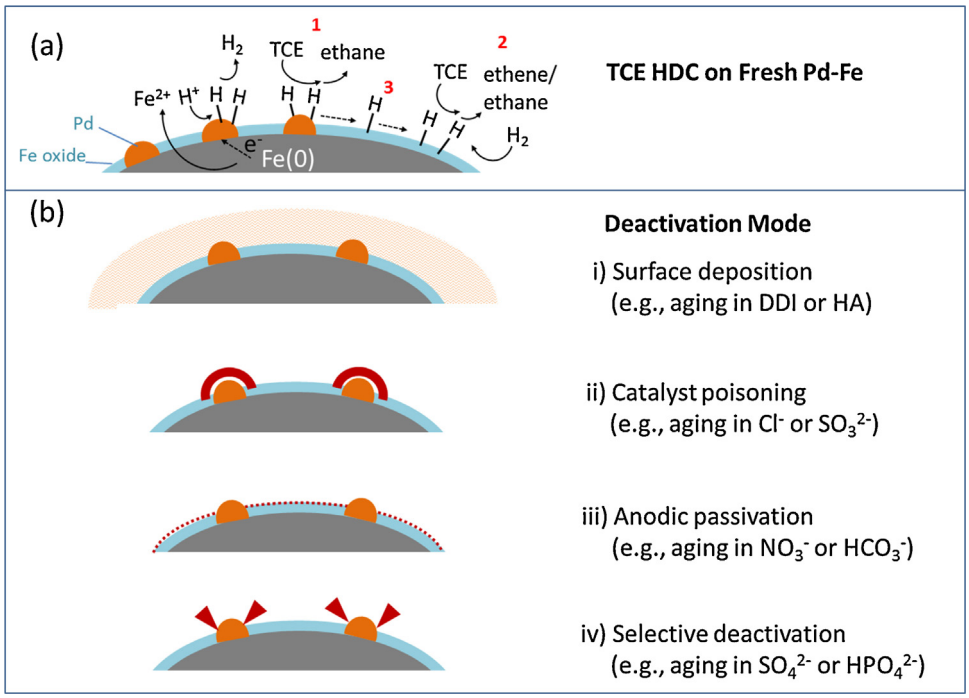

Fig. 6. Proposed mechanisms for Pd-Fe BNP deactivation in different groundwater media. (i) Surface accumulation of iron oxidation products, (ii) direct poisoning of Pd catalyst, (iii) interaction of Fe surface with passivating anions inhibiting Fe corrosion and H_2 production; and (iv) selective deactivation of hydrogenation sites.

signatures of Pd and Fe-mediated TCE reactions provide powerful insights into the reaction (and deactivation) mechanisms. For freshly prepared Pd-Fe particles, the small isotope fractionation between TCE and daughter products suggests Pd is the dominant site for TCE hydrodechlorination. Upon immersion in aqueous media with different solutes, several outcomes can be postulated. Among them, two modes of catalyst deactivation often arise in heterogeneous systems: i) physical passivation of the particles due to deposition of carbonaceous or mineral precipitates, thereby blocking access to surface reactive sites, and ii) catalyst poisoning via specific binding of solute molecules to the catalytic sites rendering partial or complete loss of reactivity to the target reagents. In the case of Pd-Fe BNPs, additional factors can contribute to the decline in TCE degradation rate. For one, since Fe serves as an electron source for hydrogen evolution, anions interacting strongly with the Fe surface can slow down TCE conversion by limiting H_2 production. On the other hand, alteration of the surface chemistry during aging may disable TCE dechlorination sites on Pd, but the catalyst may still be active for hydrogen activation. In this case, obstructing one type of reactive sites may not completely shut down the degradation process, but likely results in changes in the product distribution as well as the isotope composition of the reactants and products.

Based on the observed deactivation behavior and the perceived roles of Pd and Fe in the bimetallic structure, we attribute various solute-induced deactivations to the following scenarios (Fig. 6b). Type I deactivation involves nonselective blockage of reactive sites by surface deposits. Such process should not affect the isotope fractionation of TCE dechlorination as well as the product distribution. We reason that Pd-Fe particles aged in deionized water manifest Type I deactivation on the basis that the ε_{TCEHDC} is close to that of the fresh Pd-Fe and prior microscopic characterizations reported extensive accumulation of corrosion products as a result of accelerated corrosion [56,62]. Alternatively, if Pd poisoning is the dominant deactivation mechanism (Type II deactivation), ε_{TCEHDC} will deviate from that of the fresh Pd-Fe and the value is expected to be more negative due to the increasing role of the Fe-mediated TCE decomposition. Aging in Cl^- and SO_3^{2-} solutions falls in this category due to the large ε_{TCEHDC} values and the low selectivity for ethane in the product mixture. Although Cl^- and SO_3^{2-} are known potent poisons of Pd metal [19,20,54], the reaction rate constants (k_m) of BNPs aged in the two solutions are more than one order of magnitude higher than that of the uncatalyzed Fe. This suggests that, while both solutes may hamper the direct reaction of TCE on Pd sites, the catalyst remains (at least partially) active for hydrogen activation and contributes indirectly to the enhanced TCE degradation rates. Humic acid appears to exhibit a mixed effect of surface passivation and catalyst poisoning. This is not unexpected since the humic acid macromolecules can impose a steric blockage of access to the finely dispersed Pd deposits, and natural organic carbon has abundant organothiol groups that can form strong complexes with Pd sites [21].

Deactivation induced by immersing in HCO_3^- and NO_3^- solutions has not been carefully examined for Pd-Fe BNPs in prior studies. The particles were virtually unreactive upon aging in 5 mM of each solution for 24 h. Reducing the solute concentration to 1 mM renders the particles to be partially reactive and the isotope data suggests that the reactions involve a very small isotope fractionation effect (Fig. 5c and d). Additional experiments placing the aged particles in H_2-saturated TCE solutions recorded exceedingly rapid TCE conversion (>90% removal in 40 min), hence, HCO_3^- and NO_3^- do not act by direct inactivation of Pd sites. Instead, the two solutes likely behave as corrosion inhibitors thereby impeding the formation of H_2 as the precursor of reactive hydrogen species. This anodic passivation effect is referred to as Type III deactivation in Fig. 6b.

As an additional line of evidence, we prepared Al_2O_3-supported Pd materials. The particles were subject to the same aging treatments as those of Pd-Fe BNPs and were subsequently used in TCE dechlorination experiments in the presence of 2.5 g/L of fresh iron nanoparticles as a H_2 source (Fig. S5). The results indicate that Pd aged in sulfite and chloride solutions suffered the greatest loss of activity. Although immersion in DDI, bicarbonate, and nitrate solutions have caused severe impairment of the reactivity of Pd-Fe BNPs, these solutions only cast a moderate impact on

Al_2O_3-supported Pd. These observations are in line with the proposed mechanisms that sulfite and chloride act specifically on Pd sites, whereas nitrate, chloride and DDI solutions affect Pd-Fe via modulating Fe corrosion and H_2 production rates.

The actions of phosphate and sulfate are interesting as both solutes are hard Lewis bases and would more preferably interact with the oxide skin of the Fe(0) phase than with the Pd surface. Inspection of the isotope trends of ethane and ethene (Fig. 4c and d) suggest the existence of separate pathways to ethene and ethane formation, respectively, and ethene conversion to ethane is exceedingly slow in these systems. Previous investigations of supported Pd catalysts indicate that the active sites of ethene hydrogenation are located at the Pd-support interface, where ethene adsorbs onto the support sites receiving hydrogen spilled over from the Pd sites [63,64]. With these considerations, we surmise that sulfate and phosphate impair the particle reactivity by diverting away activated hydrogen on the Pd surface and interfering with ethene hydrogenation, both could be resulted from altering the oxide surface close to Pd deposits (Type IV deactivation).

4.2. Environmental significance

With carbon isotope analysis of TCE and its degradation products, the chemical or physical effects leading to the deterioration of TCE conversion rates were identified for Pd-Fe BNPs aged in different solution environment. This insight is of value for improved design, handling, deployment, and regeneration of BNPs for remediation of site impacted by chlorinated contaminants. For instance, aggravated corrosion of Pd-Fe in solutions of low ionic strength suggests Pd-Fe should not be synthesized and stored in an aqueous environment. Many of the common groundwater solutes as well as dissolved organic matter have been shown to cast a negative influence on the particle HDC activity. The modes of deactivation are not limited to catalyst poisoning and Fe(0) exhaustion as stipulated in previous studies [62,65,13]. As such, conventional regeneration methods (*e.g.*, acid-washing or Fe(0) regeneration with reductants) may offer limited recovery of particle reactivity. Furthermore, the bimetallic design, although elegant in theory, poses practical constraints as it requires both the Fe and Pd phases to be reactive to attain efficient hydrodechlorination performance. In reality, since Fe and Pd are sensitive to different solute environments, the bimetallic material is susceptible to deactivation in a broad range of water matrices. It should be pointed out that in the present study the dose of Pd on Fe nanoparticles is relatively high compared to typical loading in field projects (<0.5 wt%) [9,10]. Increased Pd content in the BNPs beyond an optimal range is known to exacerbate iron corrosion and decrease TCE dechlorination rates [14]. While our choice of catalyst loading is to be consistent with earlier studies to permit a fair evaluation of different bimetallic systems [66], the results may overestimate the aging effects in field conditions where a much lower Pd content is used.

Acknowledgments

The authors thankfully acknowledge financial support from Texas Tech University for faculty start-up fund and the Whitacre College of Engineering for graduate fellowship.

Appendix A. Supplementary data

Supplementary data associated with this article can be found, in the online version, at http://dx.doi.org/10.1016/j.apcatb.2016.01.047.

References

[1] I.F. Cheng, Q. Fernando, N. Korte, Electrochemical dechlorination of 4-chlorophenol to phenol, Environ. Sci. Technol. 31 (4) (1997) 1074–1078.
[2] B.P. Chaplin, M. Reinhard, W.F. Schneider, C. Schuth, J.R. Shapley, T.J. Strathmann, C.J. Werth, Critical review of Pd-based catalytic treatment of priority contaminants in water, Environ. Sci. Technol. 46 (7) (2012) 3655–3670.
[3] M.S. Wong, P.J.J. Alvarez, Y.I. Fang, N. Akcin, M.O. Nutt, J.T. Miller, K.N. Heck, Cleaner water using bimetallic nanoparticle catalysts, J. Chem. Technol. Biotechnol. 84 (2) (2009) 158–166.
[4] F. Alonso, I.P. Beletskaya, M. Yus, Metal-mediated reductive hydrodehalogenation of organic halides, Chem. Rev. 102 (11) (2002) 4009–4091.
[5] K.T. Park, K. Klier, C.B. Wang, W.X. Zhang, Interaction of tetrachloroethylene with Pd(100) studied by high-resolution X-ray photoemission spectroscopy, J. Phys. Chem. B 101 (27) (1997) 5420–5428.
[6] J.B. Hoke, G.A. Gramiccioni, E.N. Balko, Catalytic hydrodechlorination of chlorophenols, Appl. Catal. B-Environ. 1 (4) (1992) 285–296.
[7] C.B. Wang, W.X. Zhang, Synthesizing nanoscale iron particles for rapid and complete dechlorination of TCE and PCBs, Environ. Sci. Technol. 31 (7) (1997) 2154–2156.
[8] J.P. Fennelly, A.L. Roberts, Reaction of 1,1,1-trichloroethane with zero-valent metals and bimetallic reductants, Environmental Science & Technology 32 (13) (1998) 1980–1988.
[9] D.W. Elliott, W.X. Zhang, Field assessment of nanoscale biometallic particles for groundwater treatment, Environ. Sci. Technol. 35 (24) (2001) 4922–4926.
[10] F. He, D.Y. Zhao, C. Paul, Field assessment of carboxymethyl cellulose stabilized iron nanoparticles for in situ destruction of chlorinated solvents in source zones, Water Res. 44 (7) (2010) 2360–2370.
[11] G.V. Lowry, M. Reinhard, Pd-catalyzed TCE dechlorination in groundwater: solute effects, biological control, and oxidative catalyst regeneration, Environ. Sci. Technol. 34 (15) (2000) 3217–3223.
[12] T. Li, J. Farrell, Reductive dechlorination of trichloroethene and carbon tetrachloride using iron and palladized-iron cathodes, Environ. Sci. Technol. 34 (1) (2000) 173–179.
[13] Y. Xie, D.M. Cwiertny, Chlorinated solvent transformation by palladized zerovalent iron: mechanistic insights from reductant loading studies and solvent kinetic isotope effects, Environ. Sci. Technol. 47 (14) (2013) 7940–7948.
[14] Y.H. Kim, E.R. Carraway, Dechlorination of chlorinated ethenes and acetylenes by palladized iron, Environ. Technol. 24 (7) (2003) 809–819.
[15] M. Elsner, M. Chartrand, N. Vanstone, G.L. Couloume, B.S. Lollar, Identifying abiotic chlorinated ethene degradation: characteristic isotope patterns in reaction products with nanoscale zero-valent iron, Environ. Sci. Technol. 42 (16) (2008) 5963–5970.
[16] X. Liang, Y. Dong, T. Kuder, L.R. Krumholz, R.P. Philp, E.C. Butler, Distinguishing abiotic and biotic transformation of tetrachloroethylene and trichloroethylene by stable carbon isotope fractionation, Environ. Sci. Technol. 41 (20) (2007) 7094–7100.
[17] Y. Liu, T. Phenrat, G.V. Lowry, Effect of TCE concentration and dissolved groundwater solutes on NUI-Promoted TCE dechlorination and H-2 evolution, Environ. Sci. Technol. 41 (22) (2007) 7881–7887.
[18] J. Farrell, M. Kason, N. Melitas, T. Li, Investigation of the long-term performance of zero-valent iron for reductive dechlorination of trichloroethylene, Environ. Sci. Technol. 34 (3) (2000).
[19] H. Hildebrand, K. Mackenzie, F.-D. Kopinke, Pd/Fe3O4 nano-catalysts for selective dehalogenation in wastewater treatment processes-Influence of water constituents, Appl. Catal. B-Environ. 91 (1–2) (2009) 389–396.
[20] S. Ordonez, B.P. Vivas, F.V. Diez, Minimization of the deactivation of palladium catalysts in the hydrodechlorination of trichloroethylene in wastewaters, Appl. Catal. B-Environ. 95 (3–4) (2010) 288–296.
[21] F.-D. Kopinke, D. Angeles-Wedler, D. Fritsch, K. Mackenzie, Pd-catalyzed hydrodechlorination of chlorinated aromatics in contaminated waters-effects of surfactants, organic matter and catalyst protection by silicone coating, Appl. Catal. B-Environ. 96 (3–4) (2010) 323–328.
[22] B.W. Zhu, T.T. Lim, Catalytic reduction of chlorobenzenes with Pd/Fe nanoparticles: reactive sites, catalyst stability, particle aging, and regeneration, Environ. Sci. Technol. 41 (21) (2007) 7523–7529.
[23] W. Yan, A.A. Herzing, X.-Q. Li, C.J. Kiely, W.-X. Zhang, Structural evolution of Pd-Doped nanoscale zero-valent iron (nZVI) in aqueous media and implications for particle aging and reactivity, Environ. Sci. Technol. 44 (11) (2010) 4288–4294.
[24] C. Aeppli, T.B. Hofstetter, H.I.F. Amaral, R. Kipfer, R.P. Schwarzenbach, M. Berg, Quantifying in situ transformation rates of chlorinated ethenes by combining compound-specific stable isotope analysis, groundwater dating, and carbon isotope mass balances, Environ. Sci. Technol. 44 (10) (2010) 3705–3711.
[25] D. Bouchard, D. Hunkeler, P. Gaganis, R. Aravena, P. Hohener, M.M. Broholm, P. Kjeldsen, Carbon isotope fractionation during diffusion and biodegradation of petroleum hydrocarbons in the unsaturated zone: field experiment at Vaerlose airbase, Denmark, and modeling, Environ. Sci. Technol. 42 (2) (2008) 596–601.
[26] R.U. Meckenstock, B. Morasch, C. Griebler, H.H. Richnow, Stable isotope fractionation analysis as a tool to monitor biodegradation in contaminated acquifers, J. Contam. Hydrol. 75 (3–4) (2004) 215–255.

[27] F.D. Kopinke, A. Georgi, M. Voskamp, H.H. Richnow, Carbon isotope fractionation of organic contaminants due to retardation on humic substances: implications for natural attenuation studies in aquifers, Environ. Sci. Technol. 39 (16) (2005) 6052–6062.
[28] T. Kuder, P. Philp, J. Allen, Effects of volatilization on carbon and hydrogen isotope ratios of MTBE, Environ. Sci. Technol. 43 (6) (2009) 1763–1768.
[29] X. Liang, R.P. Philp, E.C. Butler, Kinetic and isotope analyses of tetrachloroethylene and trichloroethylene degradation by model Fe(II)-bearing minerals, Chemosphere 75 (1) (2009) 63–69.
[30] G.F. Slater, B.S. Lollar, R.A. King, S. O'Hannesin, Isotopic fractionation during reductive dechlorination of trichloroethene by zero-valent iron: influence of surface treatment, Chemosphere 49 (6) (2002) 587–596.
[31] M. Bill, C. Schuth, J.A.C. Barth, R.M. Kalin, Carbon isotope fractionation during abiotic reductive dehalogenation of trichloroethene (TCE), Chemosphere 44 (5) (2001) 1281–1286.
[32] M. Elsner, isotope fractionation to investigate natural transformation mechanisms of organic contaminants: principles, prospects and limitations, J. Environ. Monit. 12 (11) (2010) 2005–2031.
[33] N. Vanstone, M. Elsner, G. Lacrampe-Couloume, S. Mabury, B.S. Lollar, Potential for identifyng abiotic chloroalkane degradation mechanisms using carbon isotopic fractionation, Environ. Sci. Technol. 42 (1) (2008) 126–132.
[34] Y. Han, W. Yan, Bimetallic nickel-iron nanoparticles for groundwater decontamination: effect of groundwater constituents on surface deactivation, Water Res. (2014), under review.
[35] M. Elsner, L. Zwank, D. Hunkeler, R.P. Schwarzenbach, A new concept linking observable stable isotope fractionation to transformation pathways of organic pollutants, Environ. Sci. Technol. 39 (18) (2005) 6896–6916.
[36] J. Dai, X. Xia, Z. Li, D.D. Coleman, R.F. Dias, L. Gao, J. Li, A. Deev, J. Li, D. Dessort, D. Duclerc, L. Li, J. Liu, S. Schloemer, W. Zhang, Y. Ni, G. Hu, X. Wang, Y. Tang, Inter-laboratory calibration of natural gas round robins for delta H-2 and delta C-13 using off-line and on-line techniques, Chem. Geol. 310 (2012) 49–55.
[37] Y.Q. Liu, S.A. Majetich, R.D. Tilton, D.S. Sholl, G.V. Lowry, TCE dechlorination rates, pathways, and efficiency of nanoscale iron particles with different properties, Environ. Sci. Technol. 39 (5) (2005) 1338–1345.
[38] H. Song, E.R. Carraway, Catalytic hydrodechlorination of chlorinated ethenes bly nanoscale zero-valent iron, Appl. Catal. B-Environ. 78 (1–2) (2008) 53–60.
[39] H.S. Lancet, E. Anders, Carbon isotope fractionation in the Fischer-Tropsch synthesis of methane, Science 170 (1970) 980–982.
[40] B.L. Deng, T.J. Campbell, D.R. Burris, Hydrocarbon formation in metallic iron/water systems, Environ. Sci. Technol. 31 (4) (1997) 1185–1190.
[41] C. Schuth, M. Bill, J.A.C. Barth, G.F. Slater, R.A. Kalin, Carbon isotope fractionation during reductive dechlorination of TCE in batch experiments with iron samples from reactive barriers, J. Contam. Hydrol. 66 (1–2) (2003) 25–37.
[42] N.A. VanStone, R.M. Focht, S.A. Mabury, B.S. Lollar, Effect of iron type on kinetics and carbon isotopic enrichment of chlorinated ethylenes during abiotic reduction on Fe(0), Ground Water 42 (2) (2004) 268–276.
[43] W.A. Arnold, A.L. Roberts, Pathways and kinetics of chlorinated ethylene and chlorinated acetylene reaction with Fe(O) particles, Environ. Sci. Technol. 34 (9) (2000) 1794–1805.
[44] N. Zhang, J. Luo, P. Blowers, J. Farrell, Understanding trichloroethylene chemisorption to iron surfaces using density functional theory, Environ. Sci. Technol. 42 (6) (2008) 2015–2020.
[45] K.N. Heck, B.G. Janesko, G.E. Scuseria, N.J. Halas, M.S. Wong, Observing metal-catalyzed chemical reactions in situ using surface-enhanced raman spectroscopy on Pd-Au nanoshells, J. Am. Chem. Soc. 130 (49) (2008) 16592–16600.
[46] E.M. LaBolle, G.E. Fogg, J.B. Eweis, J. Gravner, D.G. Leaist, Isotopic fractionation by diffusion in groundwater, Water Resour. Res. 44 (7) (2008).
[47] Y.Q. Liu, G.V. Lowry, Effect of particle age (Fe-o content) and solution pH on NZVI reactivity: h-2 evolution and TCE dechlorination, Environ. Scie. Technol. 40 (19) (2006) 6085–6090.
[48] T.L. Johnson, M.M. Scherer, P.G. Tratnyek, Kinetics of halogenated organic compound degradation by iron metal, Environ. Sci. Technol. 30 (8) (1996) 2634–2640.
[49] A. Carrasquillo, J.J. Jeng, R.J. Barriga, W.F. Temesghen, M.P. Soriaga, Electrode-surface coordination chemistry: ligand substitution and competitive coordination of halides at well-defined Pd(100) and Pd(111) single crystals, Inorgan. Chim. Acta 255 (2) (1997) 249–254.
[50] B.W. Zhu, T.T. Lim, J. Feng, Reductive dechlorination of 1,2,4-trichlorobenzene with palladized nanoscale Fe-0 particles supported on chitosan and silica, Chemosphere 65 (7) (2006) 1137–1145.
[51] B.P. Chaplin, M. Reinhard, W.F. Schneider, C. Schueth, J.R. Shapley, T.J. Strathmann, C.J. Werth, Critical review of Pd-based catalytic treatment of priority contaminants in water, Environ. Sci. Technol. 46 (7) (2012) 3655–3670.
[52] B.P. Chaplin, E. Roundy, K.A. Guy, J.R. Shapley, C.J. Werth, Effects of natural water ions and humic acid on catalytic nitrate reduction kinetics using an alumina supported Pd-Cu catalyst, Environ. Sci. Technol. 40 (9) (2006) 3075–3081.
[53] F.-D. Kopinke, D. Angeles-Wedler, D. Fritsch, K. Mackenzie, Pd-catalyzed hydrodechlorination of chlorinated aromatics in contaminated waters—effects of surfactants, organic matter and catalyst protection by silicone coating, Appl. Catal. B: Environ. 96 (3–4) (2010) 323–328.
[54] Z.M. de Pedro, E. Diaz, A.F. Mohedano, J.A. Casas, J.J. Rodriguez, Compared activity and stability of Pd/Al2O3 and Pd/AC catalysts in 4-chlorophenol hydrodechlorination in different pH media, Appl. Catal. B: Environ. 103 (1-2) (2011) 128–135.
[55] G. Yuan, M.A. Keane, Catalyst deactivation during the liquid phase hydrodechlorination of 2,4-dichlorophenol over supported Pd: influence of the support, Catal. Today 88 (1–2) (2003) 27–36.
[56] R. Muftikian, K. Nebesny, Q. Fernando, N. Korte, X-ray photoelectron spectra of the palladium-iron bimetallic surface used for the rapid dechlorination of chlorinated organic environmental contaminants, Environ. Sci. Technol. 30 (12) (1996) 3593–3596.
[57] L.J. Matheson, P.G. Tratnyek, Reductive dehalogenation of chlorinated methanes by iron metal, Environ. Sci. Technol. 28 (12) (1994) 2045–2053.
[58] G.V. Lowry, M. Reinhard, Hydrodehalogenation of 1-to 3-carbon halogenated organic compounds in water using a palladium catalyst and hydrogen gas, Environ. Sci. Technol. 33 (11) (1999) 1905–1910.
[59] S.J. Teichner, Recent studies on hydrogen and oxygen spillover and their impact on catalysis, Appl. Catal. 62 (1) (1990) 1–10.
[60] W.C. Conner, J.L. Falconer, Spillover in heterogeneous catalysis, Chem. Rev. 95 (3) (1995) 759–788.
[61] S. Kovenklioglu, Z.H. Cao, D. Shah, R.J. Farrauto, E.N. Balko, Direct catalytic hydrodechlorination of toxic organics in waste-water, AIChE J. 38 (7) (1992) 1003–1012.
[62] W.L. Yan, A.A. Herzing, X.Q. Li, C.J. Kiely, W.X. Zhang, Structural evolution of Pd-Doped nanoscale zero-valent iron (nZVI) in aqueous media and implications for particle aging and reactivity, Environ. Sci. Technol. 44 (11) (2010) 4288–4294.
[63] A. Sarkany, L. Guczi, A.H. Weiss, On the aging phenomenon in Pd catalyzed acetylene hydrogenation, Appl. Catal. 10 (3) (1984) 369–388.
[64] S. Leviness, V. Nair, A.H. Weiss, Z. Schay, L. Guczi, Acetylene hydrogenation selectivity control on PdCu/Al2O3 catalysts, J. Mol. Catal. 25 (1–3) (1984) 131–140.
[65] T.T. Lim, B.W. Zhu, Effects of anions on the kinetics and reactivity of nanoscale Pd/Fe in trichlorobenzene dechlorination, Chemosphere 73 (9) (2008) 1471–1477.
[66] Y. Han, W. Yan, Bimetallic nickel–iron nanoparticles for groundwater decontamination: effect of groundwater constituents on surface deactivation, Water Res. 66 (0) (2014) 149–159.